# A Cumulus Parameterization Based on a Cloud Model of Intermittently Rising Thermals

QI HU

*Department of Soil and Atmospheric Sciences, University of Missouri, Columbia, Missouri*

(Manuscript received 6 February 1996, in final form 14 March 1997)

ABSTRACT

The author presents a cumulus parameterization that uses a cloud model that describes atmospheric convection as consisting of a sequence of intermittently rising thermals. The total mass of thermals in a convection event is determined by the amount of convective available potential energy in local soundings. In the cloud model, it is assumed that a thermal entrains environmental air only at a thin layer around the top frontier of its rising body. The entrained air mass mixes with the thermal's air and produces ''mixtures'' that then detach themselves from the thermal. This limited mixing prevents deep erosion to the thermal's buoyancy by entrainment and mixing processes. The remainder of the thermal continues rising to higher levels and forming more mixtures on its way to its own level of neutral buoyancy. The mixtures also rise or sink from the levels where they form to their level of neutral buoyancy.

Evaluation of this scheme using Global Atmospheric Research Program Atlantic Tropical Experiment data shows that the parameterized convective heating and drying rates are consistent with observations. The calculated convective precipitation also shows a distribution similar to the observed total precipitation, except at the trough of the easterly waves where calculated precipitation is smaller than observed. The capability of this scheme in describing cumulus convection is further tested in a fully prognostic one-dimensional climate model. Results from this evaluation show reasonable climatological temperature and relative humidity profiles in the troposphere.

## 1. Introduction

In the troposphere, the primary energy source is at the earth's surface where solar energy is absorbed. A portion of this energy is transformed and then transported upward, by turbulence, and used to warm the near-surface layers. These layers are also moistened by surface evaporation. In the meantime, the upper troposphere cools by atmospheric radiation and large-scale advection. This vertically heterogeneous distribution of heating or cooling and moistening or drying destabilizes the troposphere. A vertically integrated measure of this instability is the amount of the convective available potential energy (CAPE). Cumulus convection occurs as a result of this instability. Inside a cumulus cloud, air rises by converting the potential energy to kinetic energy.

Convection changes the thermal structure of the troposphere so that the CAPE is either no longer accessible (e.g., it is capped) or completely removed (Arakawa and Schubert 1974; Betts 1982; Xu and Enamuel 1989; Williams and Renno 1993). Convection removes CAPE by 1) reducing the boundary layer entropy by inducing lower entropy air from the middle troposphere into the boundary layer via updrafts and penetrative downdrafts (Fritsch et al. 1976) and 2) warming the upper troposphere by forcing subsidence in a broad region of the environment surrounding the convection. The change in the atmospheric moisture profile, through exchange of water substance between clouds and the environment, also affects CAPE through the ''virtual'' effect of moisture on temperature.

Large-scale atmospheric processes that produce CAPE also create the potential for cumulus convection, whose effect is to counteract that of the forcing processes. The CAPE in an atmospheric column remains approximately invariant over a period of time that is longer than the life cycle of individual convective events. In other words, over such a period of time, the production of CAPE by large-scale processes and the consumption of CAPE by convection *nearly* balance each other[1] (Arakawa and Schubert 1974). Cumulus parameterizations for atmospheric circulation models de-

*Corresponding author address:* Dr. Qi Hu, Department of Soil and Atmospheric Sciences, University of Missouri, Columbia, 100 Gentry Hall, Columbia, MO 65211.
E-mail: qi_hu@muccmail.missouri.edu

[1] Although the large-scale forcing may vary significantly with time and thus the associated production rate of CAPE may also, the fast process of convection with its tremendous range of intensities can consume the CAPE efficiently and make the net change of CAPE small (Lord and Arakawa 1980).

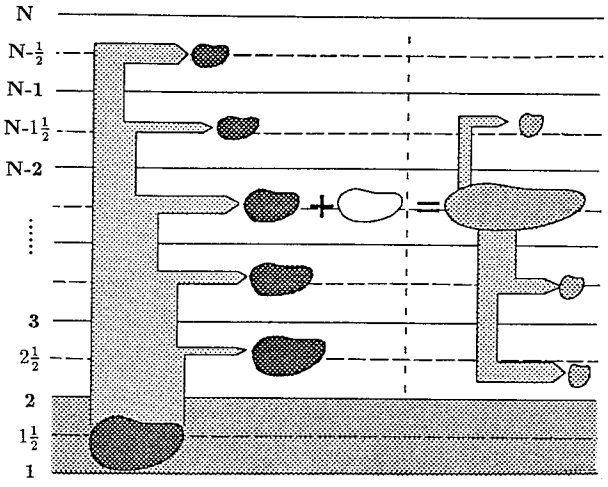


FIG. 1. Schematic illustration of the process of entrainment and mixing of a rising thermal in a discretized atmosphere. The rising thermal is shown on the left-hand side of the figure and the mixtures in a layer are shown on the right-hand side.

scribe the effect of convection in balancing the large-scale forcing and maintaining a status of invariant CAPE.

When convection develops, airflows of various scales, from turbulence to large eddies, in and around the convection, initiate entrainment and detrainment and create mixing between convective air and the environment (Betts 1973; Blyth et al. 1988; Bretherton and Smolarkiewicz 1989; Taylor and Baker 1991). If convection involves saturated elements, the mixing process can reduce the buoyancy of the cloud air very efficiently by evaporating cloud water. An example of this buoyancy reduction by mixing is shown in Fig. 1 of Kain and Fritsch (1990). Our similar calculations showed that when we changed the mixing ratio of the ambient air or slightly increased the height where mixing develops, the parcel's buoyancy became negative before the amount of the entrained environmental air reached 50% of the parcel's total mass (figures not shown). In other words, the cloud air can quickly become negatively buoyant before reaching high in the troposphere if the mixing of cloud air with environmental air is ''unrestricted.'' These calculations suggest that in the development of cumulus convection the entrainment rate of environmental air is controlled somehow by the cloud so that it can rise to the upper troposphere and induce the needed modifications and changes to atmospheric temperature and moisture profiles.

Because of our incomplete knowledge of how clouds interact with the environment, the issue of how convective clouds control their mixing remains unclear. The differences that appear in our perspectives on the development of cumulus convection and in the assumptions used in cumulus parameterizations are rooted in this lack of knowledge. Different assumptions based on theoretical considerations and on evidence from laboratory experiments and field observations have been used to limit the entrainment rate of environment air by convection. For example, in the Arakawa–Schubert parameterization the lateral entrainment rate and, hence, the potential of the mixing intensity of a developing cloud is constrained, for a particular type of cloud in a cloud spectrum, by defining the cloud top height and requiring that the entrainment and mixing process be such that when the cloud reaches that height its moist static energy is equal to that of the environment.

An alternative way of limiting erosion to cloud buoyancy by entrainment and mixing is to restrict the mixing to limited regions in a convective cloud and allow mixed regions, or ''mixtures'' to fall off the rising cloud body. Early development of this concept in cloud models was discussed and summarized by Simpson (1983). More recently, observations (Jensen et al. 1985; Blyth et al. 1988; Taylor and Baker 1991) showed that in midlatitude convection, entrainment occurs primarily at a thin layer near the top of a rising thermal. In this model of entrainment, because mixing is limited to the top thin layer of the thermal and the mixtures fall off quickly, the buoyancy of the thermal is protected from being eroded, and therefore the thermal can rise to high levels. These observations are also consistent with those of Warner (1970), who showed that the observed cloud top height often coincides with the level of neutral buoyancy calculated via the parcel method, neglecting mixing entirely.

In situ measurements near top levels of cumulus clouds of various scales show that the liquid water content of in-cloud air is highly inhomogeneous in a horizontal cloud cross section (Davies-Jones 1974; Heymsfield et al. 1978; Jensen et al. 1985). These measurements sometimes show the presence of a core possessing liquid water content the same as the adiabatic liquid water content of an air parcel rising from cloud base. The air in the core resembles many thermodynamic features of the rising thermals observed by Jensen et al. (1985) and Blyth et al. (1988). Outside this core, mixing is evident because the cloud liquid water content is much smaller than the adiabatic water content.

In this paper, we present a cumulus parameterization based on a cloud model of intermittently rising thermals. Figure 1 shows the schematic of the thermal model and the mixing process that a thermal experiences while rising. The thermal entrains environmental air only at its top frontier layer. The mixing results in ''peeling off'' the thermal's air mass and formation of cloud mixtures. Both the thermal and the mixtures will go through the buoyancy-sorting process (Telford 1975; Raymond and Blyth 1986) and rise or sink to their level of neutral buoyancy. A cloud is a collection of the thermals and their mixtures. Through their dependence on the vertical distribution of their levels of neutral buoyancy, these thermals and mixtures affect the environmental temperature and moisture.

In the next section we describe the cloud–thermal

model and a cumulus parameterization. In section 3, we present the results from an application of the scheme to the GATE [GARP (Global Atmospheric Research Program) Atlantic Tropical Experiment] data. The performance of this scheme from a fully prognostic perspective is evaluated in a one-dimensional (1D) climate model in section 4. The similarity and difference between this and other parameterizations using a similar concept are discussed in section 5. A potential application of this scheme to modeling distributions of atmospheric chemicals is also discussed in section 5.

## 2. A cloud model and the parameterization

### *a. Cloud model*

A thermal rises from a layer when it experiences positive buoyancy with respect to its environment. In this cloud model, we assume that in the course of rising, portions of a thermal's mass are shed as a result of the entrainment and mixing described earlier. To facilitate mathematical treatment, we split the process of entrainment and mixing into two subprocesses (Fig. 1): 1) separation of a portion of air mass from a thermal and 2) mixing of the shed thermal mass with the in situ environmental air mass to produce mixtures. We assume that cloud mixtures are saturated.[2] This entire process is equivalent to the entrainment of environmental air by the cloud, with the only difference being that the entrainment occurs only at the cloud top layer and the deep erosion to cloud buoyancy by mixing is limited by allowing mixtures to fall off the rising thermal. After shedding a fraction of its mass, the remainder of the thermal continues rising until it either loses its entire mass to producing mixtures or reaches its own level of neutral buoyancy. This thermal model is different from a bubble model (Scorer 1957; Ooyama 1971), which allows entrainment to occur around the whole surface of a bubble. In the following, we provide a criterion for a thermal to develop in the atmosphere and describe details of each of the two subprocesses in the life cycle of a rising thermal.

To test whether a thermal is to rise from a level, $i$, in model atmosphere, we apply the condition (Fritsch and Chappell 1980)

$$C^i = (T^i_{\mathrm{LCL}} + \Delta T^i) - T^i_e, \tag{1}$$

where $T^i_e$ is the environmental temperature at the parcel's lifting condensation level (LCL). A thermal perturbation, $\Delta T^i$, is added to the parcel's temperature at the LCL to take into account the effect of grid-scale vertical motion that may enhance the development of a thermal (Chen and Orville 1980). In the presence of grid-scale downward motion, this effect will inhibit a parcel from rising. We use a form similar to that in Fritsch and Chappell (1980) for $\Delta T^i$, that is,

$$\Delta T^i = c(w^i)^{1/3}, \tag{2}$$

where $w^i$ is the grid-scale vertical motion and $c$ is a unit conversion coefficient with an absolute value of unity. A thermal rises from level $i$ if $C^i > 0$.

When rising through model levels, the buoyancy of the thermal changes and is calculated by

$$b = g\left(\frac{\theta_v - \theta_{ve}}{\theta_{ve}} - l\right), \tag{3}$$

where $\theta_v$ and $\theta_{ve}$ are the virtual potential temperatures of the thermal and the environment, respectively; and $l$ is the mixing ratio of condensate in the thermal, representing the water loading effect on the thermal's buoyancy.

A thermal is assumed to rise dry adiabatically before saturation occurs. After saturation, we assume that the thermal conserves its equivalent potential temperature $\theta_e$ in further rising. The temperature of the thermal is calculated using iteration methods from the known $\theta$ or $\theta_e$, the mixing ratio of water vapor, and the pressure value at the thermal's height.

The detailed processes of entrainment and mixing that cause mass shedding from thermals may be modeled after knowing the turbulent nature of the flows surrounding the top frontier of the thermals. The intensity of the turbulence helps to determine the mixing length within a thermal (Stull 1984). However, these details remain unresolved both observationally and experimentally. In this model we consider the bulk effect of the entrainment and mixing and describe it through the two subprocesses outlined above. We assume that the rate of mass shed from a thermal decreases exponentially with height, that is,

$$\frac{dm}{dz} = -\frac{m}{\lambda}, \tag{4}$$

where $m$ is the mass of a thermal entering a layer of depth $dz$ and $\lambda$ is a detrainment length scale whose value will be determined later. An integration of (4) over layer depth yields the thermal's mass shed to the layer.

After a fraction of the thermal's mass is shed at layer $i$, the remainder of the thermal moves to the next layer above. The mass shed at layer $i$ mixes with the local environmental air and produces mixtures. We assume that there are a maximum of nine mixtures to form from

[2] It is true that cloudy air in the real atmosphere may not always be saturated. Walcek (1994) discussed the relative humidity criteria used in atmospheric models for separating cloudy from noncloudy air. They vary from 70% to 100%. This large difference highlights the uncertainty of what relative humidity value to use to discriminate cloudy air in the atmosphere and in models. We use 100% relative humidity for cloudy air because it is more justifiable than other values. The observations of Stith (1992) also show that the averaged liquid and/or ice water content in cloud is generally nonzero.

the mixing process.[3] All the mixtures will have an equal amount of mass from the thermal but have different fractions of environmental air. For a mixture of unit mass, for example, there will be a fraction, $f$, of mass from the environment and $(1 - f)$ from the thermal. The value of $f$ increases from 0.1 to 0.9 for mixtures 1 through 9. This treatment is similar to that of Raymond and Blyth (1986). However, we also allow the actual number of mixtures to be fewer than nine, depending on the temperature and moisture properties of the thermal's mass shed at layer $i$. This is consistent with the saturation assumption that we made for cloud mixtures.

The temperature and mixing ratios of water vapor and water condensate of each of the mixtures in a layer are calculated based on conservation relations. From water conservation we have (Walcek and Taylor 1986)

$$[q_{ad} + l_{ad}](1 - f) + q_e f = q_m + l_m, \quad (5)$$

where $q_{ad}$ and $l_{ad}$ are the mixing ratios of the thermal's water vapor and condensate, respectively. The subscript "*ad*" indicates a cloud quantity in an adiabatic process, and "*e*" indicates an environmental quantity. The terms on the right-hand side (rhs) of (5) are mixing ratios of water vapor and water condensate of a mixture, indicated by the subscript "*m.*" The conservation of energy is written

$$c_p[T_{ad}(1- f) + T_e f] = c_p T_m + L\Delta l, \quad (6)$$

where $T_{ad}$ is the thermal's temperature. The second term on the rhs of (6) is the energy used to evaporate water condensate during mixing. Because $\Delta l$ can be written as (Walcek and Taylor 1986)

$$\Delta l = l_{ad}(1 - f) - l_m, \quad (7)$$

(5) and (6) can be reorganized into

$$c_p T_m + L q_m(T_m, p) = F \quad (8)$$

and

$$l_m = [q_{ad} + l_{ad}](1 - f) + q_e f - q_m (T_m, p). \quad (9)$$

In (8),

$$F = (c_p T_{ad} + L q_{ad})(1 - f) + (c_p T_e + L q_e) f \quad (10)$$

and can be calculated before the mixing. We can solve (8) and (9) (Walcek and Taylor 1986) for temperature $T_m$ and water condensate mixing ratio $l_m$ of a mixture. The mixture's water vapor mixing ratio $q_m$ can be calculated from the above with the assumption that the mixture is saturated.

After knowing the thermodynamic properties of each of the mixtures, we examine their buoyancy. The same condition (1) is used in this test. If a mixture is positively buoyant within its environment, it will rise. Otherwise, the mixture stays at the mixing level, or sinks if its level of neutral buoyancy is below the level where the mixture is produced. When a mixture rises, it may produce precipitation. A rising mixture is, however, assumed not to shed mass as a thermal does (Raymond and Blyth 1986; Emanuel 1991).

### *b. The parameterization*

We now apply this cloud model to parameterizing cumulus convection in the troposphere. A key issue in cumulus parameterization is to determine the cloud mass flux and its vertical distribution. In the following, we describe how these are determined in this scheme.

In this scheme, cumulus convection is considered to consist of a sequence of *thermal events.* One thermal event is defined to consist of all the individual thermals detected by (1) at all the model layers in one scan from the lowest layer up through the layer next to the top model layer. For example, when there are $N$ layers in the model atmosphere (Fig. 1) there are possibly 0 to $N - 1$ thermals in one thermal event; a thermal may rise from each layer, except for the top layer. To allow updraft air to originate from multiple model layers is one of the unique features of this parameterization. It will be useful in describing and understanding convective transport and redistribution of atmospheric chemicals. We will further discuss this issue in section 5.

In a thermal event, the upward convective mass flux across a model level is the summation of the mass flux of all the individual thermals and the rising mixtures that penetrate through that level. Similarly, the downward convective mass flux across a model level is the summation of mass fluxes of the mixtures that are produced by thermals in the thermal event and sink through that level.

We calculate the upward and downward mass fluxes of one thermal event in the following way. First, we assume that each thermal in the thermal event has a unit amount of mass (1 kg). Then, we normalize the total mass of all thermals in the thermal event. For example, if there are two thermals rising from two different layers, each of the thermals will initially have 1 kg of mass. Then, after the normalization, each will be reassigned 0.5 kg of mass if the two layers have equal amounts of total air mass in a grid area. If the vertical discretization in a model is such that the two layers have different amounts of total air mass at a grid area, the total mass of the two thermals will remain unity, but each thermal's air mass will be different and determined using the mass-weight average method. The layer with a larger amount of total air mass will give rise to a larger thermal. The same method applies to multilayer situations.

Knowing the mass amount of thermals rising from different layers in a model we calculate, using the formula in section 2a, the amount of mass shed by the thermals and the mass of mixtures in each layer in the model atmosphere. After the buoyancy sorting over the mixtures we obtain the upward and downward mass fluxes across the boundaries of each model layer. Con-

[3] It would be ideal to allow a larger number of mixtures to form from the mixing process. The calculations can become very involved when the number increases, however.

tinuity of mass is used to determine the amount of subsiding air mass across the boundaries.

From the mass flux profiles we evaluate the effect of the thermal event on changes of temperature and moisture at each of the model layers. We use the mass-weight average over all the mass elements that a layer is composed of after the vertical mass redistribution in one thermal event. The updated profiles of temperature and moisture are used to calculate new CAPE values and to determine whether the next thermal event is necessary.

A *convection episode* is composed of all the thermal events necessary to remove the CAPE in a local sounding. Accordingly, the total mass fluxes of a convection episode are summations of the convective mass fluxes of all the thermal events. The changes of temperature and moisture due to convection are calculated from differencing the initial sounding and the final sounding when CAPE is removed.

In mathematical form, the time rate of temperature change of a layer due to convection is described as

$$\frac{\partial T}{\partial t} = \int_{(m)} \left( -\frac{\partial \overline{\omega' T'}}{\partial p} + R\frac{\overline{\omega' T'}}{c_p p} - \frac{L(E - P)}{c_p} \right) dm, \quad (11)$$

where the first two terms in the integral are contributions of individual thermals and $L(E - P)/c_p$ is the net heating due to condensation. The integral is over all the thermal events constituting the convection episode. In discretized form, (11) is a summation of changes of temperature due to individual thermal events. The temperature change of a layer of a grid area in one thermal event can be written as

$$\begin{aligned}\left(\frac{\Delta p^i}{g}\right)\Delta T^i = &\sum_{r=1}^{i-1} \left\{ \sum_{k}^{\{K_1\}} \mathrm{DTRN}^{r,i,k} T(\theta_e^{r,i}, q_{ad}^{r,i}) \right. \\ &\left. - \sum_{k'}^{\{K_2\}} \mathrm{ETRN}^{r,i,k'} T(\Theta_e^i, q_e^i) \right\} \\ &+ \sum_{r=1}^{N-1} \sum_{j=r+1}^{N} \sum_{k=1}^{K} [m_s^{r,j,k,i} T(\theta_{e_s}^{r,j,k,i}, q_{s\_ad}^{r,j,k,i})] \\ &- m_u^i \Theta_e^i - m_{sub}^i \left(\frac{\partial \Theta_e}{\partial p}\right)^i \Delta p^i - LE^i. \quad (12)\end{aligned}$$

In (12), $\Delta p^i/g$ is the total air mass of layer *i*. On the rhs of (12), $T(\theta_e, q)$ is a temperature of a thermal obtained iteratively from known $\theta_e$ and water substance quantities, $q$, in thermals and mixtures. In the summations, $\{K\}$ is the total number of mixtures resulted from mixing of the shed mass of a thermal and the environmental air mass in layer *i*. Among these mixtures some will have their level of neutral buoyancy in layer *i*. These mixtures will stay at the layer. We group these mixtures into $\{K_1\}$. The rest of the mixtures will have their level of neutral buoyancy in layers different from layer *i*. These mixtures will leave the layer and undergo further rising or sinking. They are grouped in $\{K_2\}$. Because the effects of the mixtures in these two groups on mass exchange and temperature change of layer *i* are different, they are treated separately in (12). The superscripts from left to right, for example, *r, j, k,* and *i,* of a quantity describe the history and the future of a mixture and are defined as follows. The first one from the left specifies the index of the layer from where a thermal originates; the second specifies the index of the layer where this thermal sheds a fraction of its mass; the third specifies the rank of a particular mixture in all the mixtures formed; and the fourth tells the index of the layer where the mixture has its level of neutral buoyancy. For the case when three superscripts are present, they have the meanings of the first three superscripts from the left, and so forth.

The first term under the brace parentheses on the rhs of (12) describes the effect on temperature from mass exchange between layer *i* and the thermals rising from layers below. In this term, ''DTRN'' is the mass amount that thermals deposit to layer *i* and ''ETRN'' is the mass of the layer that will leave the layer in the form of mixtures. The environmental air's equivalent potential temperature in layer *i* is $\Theta_e$ and its mixing ratio is $q_e$.

The second term on the rhs of the equation describes contributions from all the mixtures that are produced at layers different than layer *i* but whose level of neutral buoyancy is in layer *i*. The effect on temperature change due to the air mass leaving layer *i* as a thermal is taken into account in the third term. The fourth term is the compensating subsidence effect on temperature change. In this term, $m_{sub}$ is the subsiding air mass entering layer *i*. The last term describes cooling effect due to reevaporation of rain passing through the layer. In (12), the condensation effect that drives the thermals to rise to layer *i* is included in the first two terms on the rhs.

By analogy, the total change of moisture of layer *i* in one thermal event is calculated from

$$\begin{aligned}\left(\frac{\Delta p^i}{g}\right)\Delta q^i = &\sum_{r=1}^{i-1} \left\{ \sum_{k}^{\{K_1\}} \mathrm{DTRN}^{r,i,k} \left[ q_{ad}^{r,i} + \sum_{n=r}^{i} (1 - \epsilon^i) l_{ad}^{r,n} \right] - \sum_{k'}^{\{K_2\}} \mathrm{ETRN}^{r,i,k'} q_e^i \right\} - m_{sub}^i \left(\frac{\partial q_e}{\partial p}\right)^i \Delta p^i \\ &+ \sum_{r=1}^{N-1} \sum_{j=r+1}^{N} \sum_{k=1}^{K} \left\{ m_s^{r,j,k,i} \left[ q_{s\_ad}^{r,j,k,i} + \sum_{n=j}^{i} (1 - \epsilon^i) l_{s\_ad}^{r,j,k,n} \right] \right\} - m_u^i q_e^i + E^i. \quad (13)\end{aligned}$$

Here, the symbols are similar to those in (12). The total change of temperature and moisture in layer $i$ due to convection in a convection episode is obtained by summing (12) and (13), respectively, over all thermal events in the convection episode.

The total precipitation of a convection episode consists of precipitation from all individual thermal events. The form of the precipitation can be either liquid or solid, depending on whether the parcel's temperature is below the freezing temperature. The reevaporation of falling precipitation is calculated from

$$E(m_r) = \alpha q_{\text{sat}}(1 - \text{RH}) m_r^{\beta} t. \tag{14}$$

Here, the values of $\alpha$ and $\beta$ are 0.0485 and 0.65, respectively (Yamasaki 1975); and $m_r$ is the mass of rain water. In (14), RH is the environmental relative humidity (relative to either rain or ice); $t$ is the time period when rain falls through a layer and is dependent on the terminal velocity of falling precipitates, which is calculated from

$$V_T = \eta m_r^{\zeta}. \tag{15}$$

Here, $\eta$ and $\zeta$ are 12.2 and 0.125, respectively, and are also from Yamasaki (1975). At present, we ignore the differences in the terminal velocities between solid and liquid precipitates. The total precipitation reaching the ground is the total rainwater less the reevaporated amount:

$$P = \sum_{\{\text{event}\}} \sum_{i=1}^{N} \left( \sum_{j=1}^{i} \epsilon l_{ad}^{j,i} m_u^{j,i} + \sum_{r=1}^{N-1} \sum_{j=r+1}^{N} \sum_{k=1}^{K} \epsilon l_{s\_ad}^{r,j,k,i} m_s^{r,j,k,i} - \sum_{j=i}^{1} E_j(\sigma m_p^i) - \sum_{j=b}^{1} E_j[(1 - \sigma) m_p^i] \right). \tag{16}$$

In (16), the first summation is over the number of thermal events that constitute the convection episode. The second summation is over all the model layers where thermals and mixtures produce precipitation. Inside this summation, the first two terms are rainwater amounts at layer $i$ produced by thermals and mixtures, respectively. The parameter $\epsilon$ is the precipitation efficiency. The superscripts have the same meanings as those described earlier. The last two terms in the parentheses represent reductions by reevaporation of precipitation falling from the layer $i$. In these two terms, $m_p^i$ is the rain amount at the layer $i$ (equivalent to the summation of the first two terms in the parentheses). The parameter $\sigma$ is the faction of rain available for reevaporation above the cloud base $b$. Below the cloud base, all rain water is subject to reevaporation. If we assume that rain does not evaporate inside clouds, $\sigma$ serves as a probability measure of the likelihood for rain to fall outside of a convective cloud.

The parameter $\sigma$ is set to be 0.15 above the cloud base. Our justification for using such a value is based on the observation that convection often tilts even in weak shear conditions. If we assume that an averaged vertical tilt in weak shear is around 10° [see the schematic in Emanuel (1983)] and that the condensate is uniformly distributed in a horizontal cross section of a thermal, the vertically averaged fractional area of the cross section projected outside the cloud base area on the ground surface is around 0.15. Condensates in this fractional area will fall outside of the thermal for reevaporation. This is a crude estimation but it should be in a reasonable range of the values.

When individual thermals and mixtures have condensate, the amount of condensate that rains is determined by the precipitation efficiency $\epsilon$. Cloud precipitation efficiency is a complex function of three-dimensional interactions involving motions of scales ranging from microscale (e.g., the process that affects the cloud microphysics) to mesoscale (e.g., the organization of updrafts and downdrafts in cumulus convection). One of the important dynamic factors that affect precipitation efficiency is the vertical wind shear in the cloud and around its environment. Observations, as summarized in Fig. 2 of Fritsch and Chappell (1980), show the relationship between the two. In this scheme, because dynamics are not included, a value must be chosen for $\epsilon$. Consistent with our philosophy that convection in a strongly sheared environment can be best described only with fully invoked mesoscale and cloud dynamics, we choose a precipitation efficiency of 90%.

As discussed in the previous section, the large-scale atmospheric processes produce CAPE and thus create the potential for cumulus convection, whose effect is to remove the CAPE. Because cumulus convection can have a tremendous range of intensities and is very efficient at removing CAPE in a sounding, we assume in this scheme that within a given period of time the CAPE created by forcing processes is nearly balanced by CAPE removal by convection. This is similar to the quasi-balance assumption proposed by Arakawa and Schubert (1974). Based on this assumption, when applying this scheme in an atmospheric model we will have the quasi-balance condition at the end of each time step. Convection, in terms of a sequence of thermal events, develops to remove the CAPE produced by forcing processes within the time step. The changes of temperature and moisture due to convection in one time step are calculated by summation of (12) and (13), respectively, over all the thermal events necessary to remove the CAPE. The total precipitation in the time step is computed from (16).

In executing the scheme, it usually takes a long time to remove a certain amount of CAPE from a sounding when only 1-kg air mass is moved by thermals in every thermal event. To ensure that the quasi-balance between large-scale forcing and convection is reached within a nominal model time step, we modify the convective mass in a thermal event as follows. After the buoyancy sorting, and before calculating the properties of thermals and mixtures in a thermal event, we calculate the total

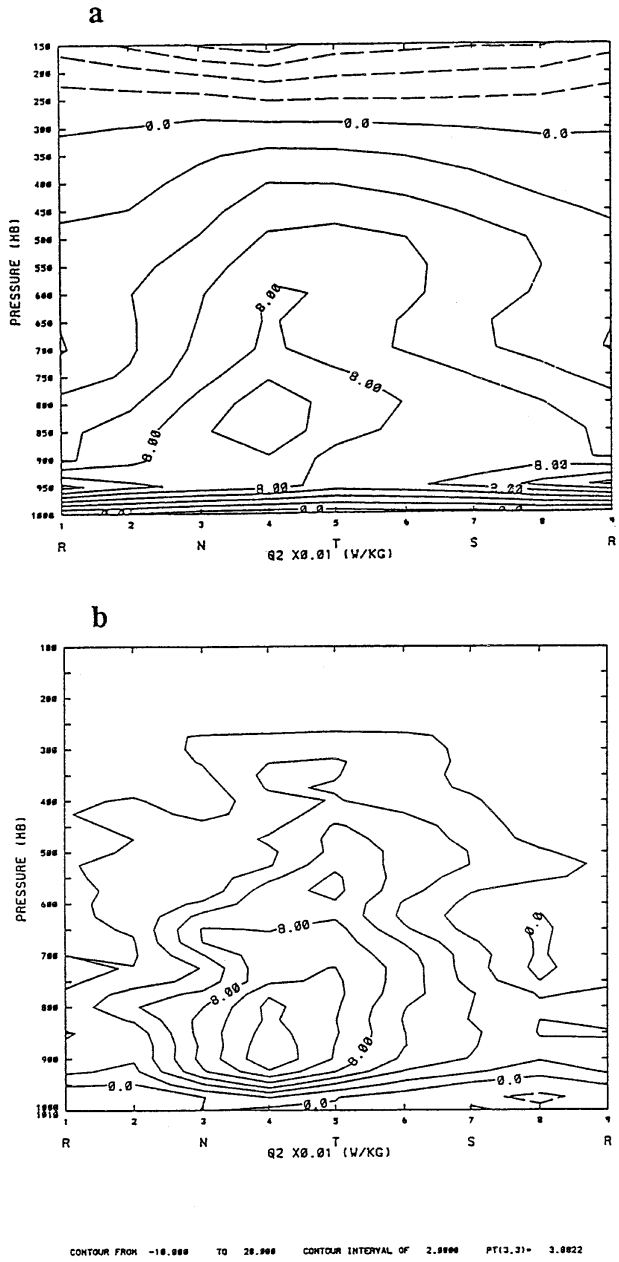


FIG. 2. Composites of convective drying (a) calculated using the scheme and (b) diagnosed from observation (in units of 0.01 W kg$^{-1}$). Contour interval is $2 \times 10^{-2}$ W kg$^{-1}$. The calculated maximum drying rate is $11.8 \times 10^{-2}$ W kg$^{-1}$. The GATE wave positions are marked on the abscissa (see text).

amount of mass exchange in each layer of the model and find the layer that observes the maximum amount of mass exchange with the thermals and mixtures. We adjust the normalized mass of the thermal event so that this maximum mass exchange amount is equal to, or less than (e.g., in the last thermal event), 5% of the total mass of that layer of a grid area. By multiplying the mass amount of every thermal in the thermal event and the mixtures by this factor we obtain the total convective airmass and mass flux profiles in the thermal event, which will then be applied in (12), (13), and (16).

In fact, because the thermal effects are repeated in thermal events in the scheme until CAPE is removed, we will get the same net heating or drying tendencies and total precipitation when we use 1-kg air mass or a modified value of it. This 5% value is selected to ensure the computation is stable and the final results will not be rendered.

In the next two sections we evaluate this cumulus parameterization.

## 3. Calculation of GATE profiles

The GATE observations provide a comprehensive dataset of tropical wave disturbances and convection and have frequently been used in evaluating convective parameterizations (Lord 1982; Betts and Miller 1986; Tiedtke 1989; Randall and Wang 1992). In this section, we apply our convective scheme to the GATE data and compare parameterized convective heating or drying rates and precipitation amount to those observed.

The GATE data that we use contain soundings in 3-h intervals from 0000 UTC 30 August to 2100 UTC 18 September 1974 during Phase III of GATE (Thompson et al. 1979). In our calculation, we divide each 3-h period into three subperiods of 1 h and apply the same forcing tendencies in the three 1-h periods. The scheme is applied in each 1-h period to calculate convective mass fluxes, convective effects on temperature and moisture, and precipitation. At the end of each hour we update the sounding by adding to it the diagnosed forcing tendencies due to large-scale processes to prepare for the following step convection calculation. This procedure is similar, to some extent, to that described by Lord (1982), who updated the sounding every 3 h. After finishing the calculation in the GATE period, we composite the convective heating and drying according to the phase of the easterly waves.

We used the observed vertical motion (Thompson et al. 1979) at each time step for $w$ in (2). The value of $\lambda$ used in (4) is 2000 m. This value is used based on the diagnostic profile of entrainment rate from the Marshall Island data [Fig. 14 of Yanai et al. (1973)]. Yanai et al. (1973) showed that the environmental air mass entrained and mixed into clouds is large in the lowest 2000 m and decreases rapidly upward. This result may be interpreted from our thermal model's viewpoint as that more mass of rising thermals mixes with the environmental air in low levels than in high levels. Equivalently, this is saying that more of a thermal's mass will be shed in the low levels and mix into cloud mixtures. As such, the vertical profile of the mass shedding of a thermal will have a close-to-exponential shape as shown in Yanai et al.'s Fig. 14.

Figure 2 shows calculated and observed composites of convective drying rate at different phases of easterly waves in GATE. The upper panel is the parameterized

result and the lower panel is diagnosed by Thompson et al. (1979). On the abscissa, ''R'' is the ridge location of the composite wave, ''N'' is the northerly flow region ahead of a westward propagating trough marked by ''T,'' and ''S'' is the southerly flow region behind the trough. The calculated drying rate and distribution are consistent with their observed counterparts. In Fig. 2a, a large convective drying region is between the trough and the northerly flow from 900 to 750 hPa. A similar drying exists in Fig. 2b although the maximum drying rate from the scheme is not quite as large as the observed. The feature of a double layer of drying from the trough location to the southerly flow region observed in Fig. 2b is also depicted in Fig. 2a.

A major difference between Figs. 2a and 2b is that the calculated result has a large drying rate in the layers below 800 hPa compared to that in Fig. 2b, particularly around the ridge of the waves. This difference could partially be due to the fact that we have required a removal of *all* CAPE from the sounding. In reality, after convection and around the ridge of the waves, a relatively dry atmosphere favors surface evaporation, which moistens the low layers and helps the development of the atmospheric boundary layer after convection (Sarachik 1976). A finite amount of CAPE is present in this boundary layer development process. In addition, there is possibly nonzero background CAPE in the atmosphere (Williams and Renno 1993). Removing all the CAPE and, hence, maintaining a strictly neutral atmosphere in this parameterization may have converted those CAPE units into convection activity and caused the excessive drying in the boundary layer. We enforce the zero CAPE condition in this calculation because what the minimum CAPE value should be is uncertain (Emanuel et al. 1994).

Another potential cause for the extra dryness in the boundary layer in Fig. 2a is the exclusion of penetrative downdrafts (Fritsch et al. 1976; Raymond 1995) in this parameterization. The effect on the results of this parameterization from not including these downdrafts will be further discussed in section 5.

The calculated composite convective heating rate in the atmosphere is shown in Fig. 3a. It compares favorably to the diagnosed heating structure in Fig. 3b. The level of maximum heating rate is at 600 hPa in both panels. The calculated heating rate has a broad center of $12 \times 10^{-2}$ W kg$^{-1}$ ahead of the trough. A similar heating rate is found at the trough location in the observation. In Fig. 3b, the heating around the ridge and in the southerly flow is more intense than the calculated result, however. This diagnosed convective heating structure is not well in phase with the easterly waves as suggested by wave study results (Reed and Recker 1971). This is primarily because the GATE experiment took place near the monsoon trough region of the ITCZ where the trade wind convergence and associated large scale circulations contributed significantly to convection development in the experiment.

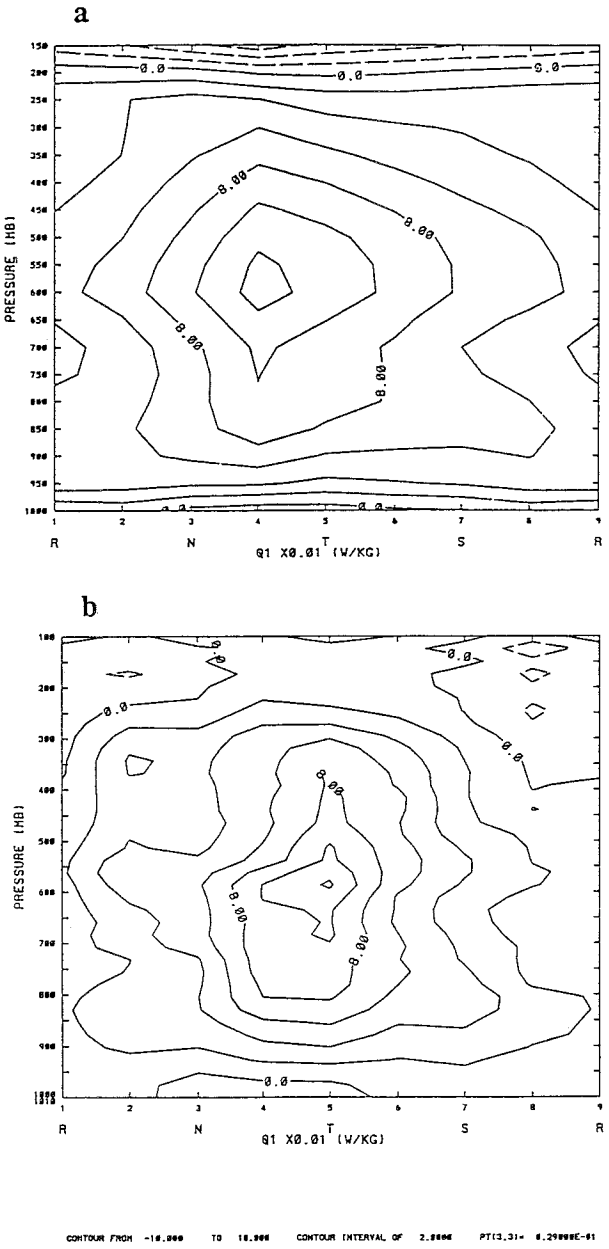


FIG. 3. Composites of convective heating (a) calculated using the scheme and (b) diagnosed from observation (in units of 0.01 W kg$^{-1}$). Contour interval is $2 \times 10^{-2}$ W kg$^{-1}$. The calculated maximum heat rate is $13.3 \times 10^{-2}$ W kg$^{-1}$.

That the parameterized heating is more in-phase than the diagnosed heating with the easterly waves may be interpreted as follows. The diagnosed vertical motion in GATE (Fig. 14 of Thompson et al. 1979) has a maximum upward vertical motion at 800 hPa *ahead* of the trough location. The maximum heating in the parameterized result coincides with this maximum upward vertical motion. That the diagnosed maximum heating is about 45° *behind* the maximum upward vertical motion suggests that large-scale circulations play a role in de-

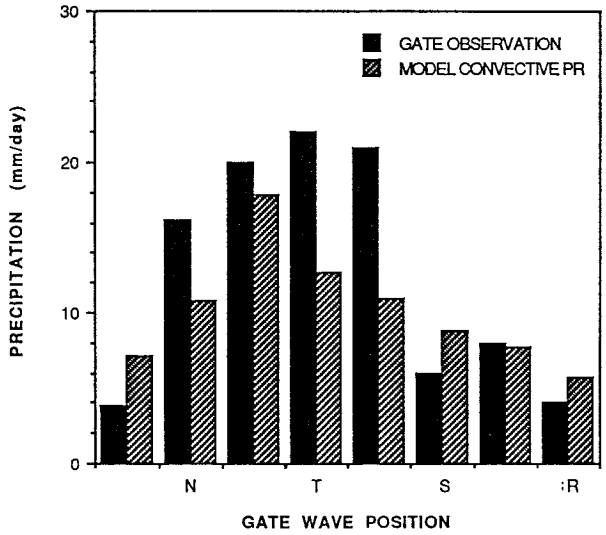


FIG. 4. Histogram of composites of calculated convective precipitation and observed total precipitation during GATE. The abscissa shows the wave positions.

termining the diagnosed heating structure. A strong westerly wind existed through the troposphere above 800 hPa from wave location ''N'' to the ridge (Fig. 11a in Thompson et al. 1979). The dynamic effects of this westerly wind seems significant on the location of the observed maximum convective heating. These dynamic effects cannot, however, be included in the large-scale forcing tendencies used in calculation of convective heating. This may have caused the discrepancy in the phase relation.

Figure 4 shows the composite convective precipitation from the parameterization and the composite of the observed daily total precipitation. The calculated convective precipitation increases from ridge to trough and reaches a maximum before the trough, consistent with the drying and heating structures in Figs. 2a and 3a. The observed total precipitation has maximum intensity at the trough. The calculated amount is smaller than the observed in the northerly flow and trough regions and is larger than the observed in the other regions of the easterly waves. We recall that the observed total precipitation is an average over the stations in the B-scale area in GATE (Thompson et al. 1979). The parameterized precipitation used forcing tendencies derived from stations' data covering a much larger area (the A–B-scale region in GATE). The tendencies averaged over such a larger area might have caused underestimate of the forcing driving the precipitation development during the passage of troughs in the smaller B-scale region.

## 4. Performance of the scheme in a 1D model

### *a. Model and results*

To evaluate this parameterization from a prognostic perspective we implemented it in a simple 1D climate model. In this model, the atmosphere extends from sea level at 1006 hPa to the model top at 100 hPa, where a rigid-lid upper boundary is assumed. A fixed sea surface temperature (SST) of 301.65 K is assumed to be the lower boundary of the atmosphere. The vertical domain of the model is divided into 15 $\sigma$ layers[4] bounded by 16 $\sigma$ values (1.0, 0.99, 0.98, 0.96, 0.93, 0.89, 0.84, 0.78, 0.70, 0.60, 0.50, 0.40, 0.30, 0.20, 0.10, and 0.0).

In the model, the temperature and water vapor and liquid water mixing ratios are evaluated at the center level of each layer. A linear interpolation based on log-pressure is used to calculate the values of these quantities at interfaces between two adjacent layers. The surface fluxes of moisture and sensible heat are calculated using the bulk aerodynamic formulas

$$E = \rho_0 c_D |\mathbf{V}|[q^*(\mathrm{SST}, p_0) - q_1] \tag{17}$$

and

$$H = c_p \rho_0 c_D |\mathbf{V}|(T_s - T_1), \tag{18}$$

respectively. In the above, $q^*$ is the saturation vapor mixing ratio at the SST and the sea level pressure; $T_s$ is the air temperature at the surface level and is assumed to be equal to the SST; and $q_1$ and $T_1$ are the water vapor mixing ratio and temperature of the air, respectively, at the center of the first layer. The other symbols in (17) and (18) are $\rho_0$ the air density at the surface level, $c_D$ the surface drag coefficient, and $\mathbf{V}$ the wind at the near surface level. We use $c_D = 0.0015$ and a fixed surface wind speed of $|\mathbf{V}| = 5$ m s$^{-1}$.

Besides the surface energy fluxes, we also include in the model the effects of atmospheric radiation and large-scale advection. Because of a lack of a natural way to provide a large-scale advection tendency consistent with the other forcing processes in the model, we combine the effects of both advection and radiation on temperature into one and specify it by a constant cooling rate of 2.2 K day$^{-1}$. This is a crude assumption but is reasonable from a scaling point of view in the 1D model setting. We neglect moisture change due to large-scale advection after assuming that it is a minor effect compared to the surface moisture flux.

Vertical eddy transport processes are not explicitly described in the model. Heat and moisture in the lower atmosphere accumulated from surface fluxes are distributed in the lowest 2000-m depth following a specified exponential profile with an *e*-folding scale of 500 m.

The model parameters in the calculation use the same values as in the previous section. The only exception is that we allow a nonzero minimum CAPE of 50 J kg$^{-1}$ in the model atmosphere. This is based on the following two facts. 1) The reduction of CAPE by convection from a large value ($\sim 10^3$ J kg$^{-1}$) to this value is very efficient,

[4] This scheme was originally designed to be used in the Penn State/NCAR Mesoscale Model (MM4), which uses a terrain following $\sigma$-coordinate.

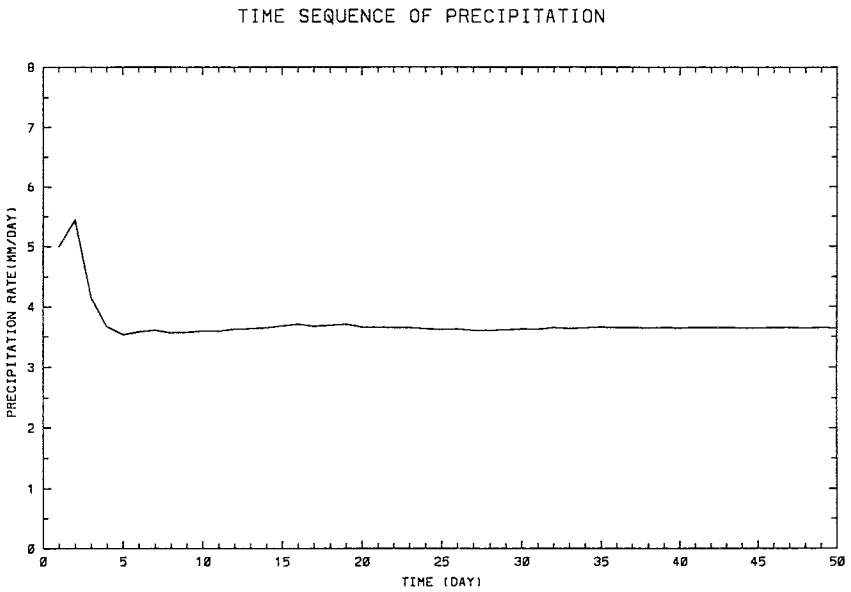


FIG. 5. Time series of convective precipitation (mm day$^{-1}$) from the 1D model.

and 2) further reduction of CAPE from this value to zero is inefficient. In many cases, it is impractical in the sense that when the CAPE is around this value, continuous thermal events of very small airmass amount result in only small fluctuations, rather than in net reductions of CAPE in the model atmosphere. A possible explanation for these modeling facts is that the absence of interactions between atmospheric dynamics and cumulus convection in the model affects the CAPE removal by convection. This will be further discussed in the next section.

We integrate the model using a time step of 30 min. The tendencies of change of temperature and moisture due to radiation, advection, and surface fluxes are updated to the sounding at the beginning of each time step. The integration was made for 100 days.

Figure 5 shows the time sequence of model precipitation rate during the first 50 days. The precipitation variation in the second 50-day period is similar to that in the last 15 days in Fig. 5. An equilibrium state was reached after about 20 days in this case. Precipitation rate at equilibrium is 3.7 mm day$^{-1}$. A continuous precipitation in the model is necessary to maintain a heat balance, particularly in the upper troposphere, in the presence of a cooling process.

The variation of temperature ($T$) and dewpoint ($T_d$) profiles during the first 50 days of integration are plotted in the skew $T$–log $p$ diagram in Fig. 6. The initial $T$ and $T_d$ profiles, taken from the GATE trough sounding, are shown by the thick dashed curves in the figure. The soundings of the model atmosphere during the integration gradually approach to a stable profile, as illustrated by the soundings at day 10 and 20 in Fig. 6. The $T$ profile at day 20 has a lapse rate between the dry and moist adiabats below 450 hPa, and it follows the moist adiabat in the layers above. Both $T$ and $T_d$ profiles on day 21 through day 100 coincide with those at day 20.

The relative humidity profile averaged over the last 5 days in the 100-day integration is shown by the solid curve in Fig. 7. The air is saturated in the top three layers above 350 hPa. In the near surface layers the relative humidity increases from 67% at 1006 hPa to 71% at about 950 hPa. Above 950 hPa, a layer of approximately uniform relative humidity of 71% extends to 900 hPa. The relative humidity starts decreasing above 900 hPa and reaches a minimum value of 48% at 600 hPa.

The saturation in the upper troposphere is due to the limitation of model dimension because there is no advection of moisture in the 1D model. Deep convection usually results in saturation in the upper troposphere because of detrainment of cloud water at cloud top. In addition, because the air in the upper troposphere is very cold and has very large specific volume, a small amount of warm and moist cloud air can result in saturation of a large volume of the in situ air by mixing. This is especially the case when convective overshooting is allowed as it is in this scheme. In the presence of persistent convection it is reasonable to have a saturated ''anvil layer'' (Randall et al. 1989) in the upper troposphere. A similar saturation layer in the upper part of the troposphere was also observed in other 1D climate models results (e.g., Emanuel 1991).

Figure 8a shows the profiles of DTRN and ETRN at the model equilibrium state. Recall that ETRN of a layer is the environmental air mass leaving a layer after participating in the mixing process and forming mixtures whose level of neutral buoyancy is at a different layer, and DTRN of a layer is the mass of mixtures that stays at the layer where their level of neutral buoyancy is.

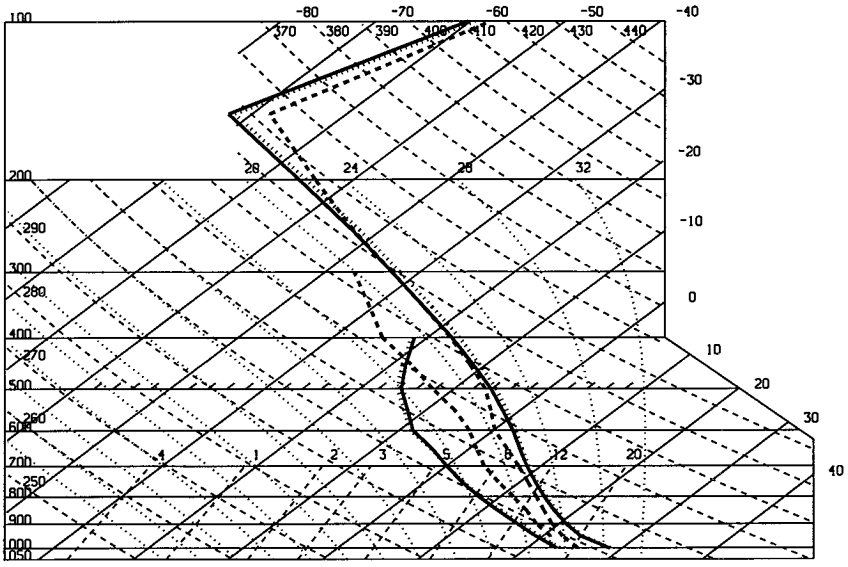

FIG. 6. Initial $T$ and $T_d$ profiles (thick dashed curves) used in 1D model integrations. Also shown are the variations of $T$ and $T_d$ profiles at day 10 (dotted) and day 20 (thick solid) in the control case.

The results in Fig. 8a show that a large amount of mass enters convection from the layers below 900 hPa and that there are no thermals whose level of neutral buoyancy is below 950 hPa. Above 950 and below 500 hPa there exists a layer of substantial DTRN. In particular, in the layers between 900 and 650 hPa the DTRN is larger than ETRN, indicating more convective air mass and cloud mixtures finding their level of neutral buoyancy in those layers. This result is consistent with the downward mass flux profile in Fig. 8b, which shows a large downward mass flux at a level just above 800 hPa and a rapid decrease of the mass flux below 800 hPa. Because cloud mixtures usually contain more moisture than the environmental air does, the lower layers in the troposphere become moister than the middle layers when more mixtures move away from the middle layers and rest at the lower layers. This explains the existence of a large relative humidity layer below 900 hPa and a dry layer at the middle troposphere from where the mixtures depart (Fig. 7).

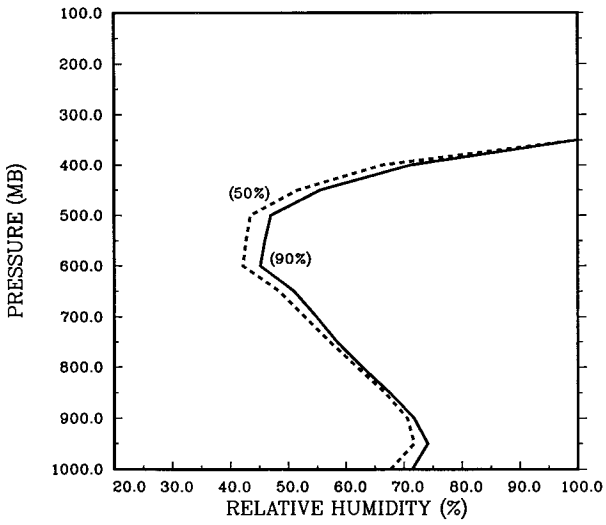


FIG. 7. Relative humidity profile at the equilibrium state from the control case (solid curve). The dashed curve is the relative humidity profile from the experiment, assuming 50% of cloud condensate falls as rain.

The ETRN rate is also large around 250 hPa where the air is saturated. Large ETRN rate around 250 hPa has a contribution from local mass overturning within the saturated layers. In these saturated layers, the lapse rate needs to be small in order to be convectively neutral or stable. Because convection is the only process in the model that can change the temperature in those high altitude layers to balance the radiation effect, a local mass overturning seems inevitable in those saturation layers. This indicates that the large-scale dynamic processes should be explicitly included in full evaluations of a convection parameterization. This result also suggests that the anvil clouds resulting from deep convection could be convectively unstable. A local mass overturning may break the anvils. In this model, because of the steady convection this breakup is prevented from occurring. The large detrainment in the top layer of the model is required by the mass conservation among entrainment and detrainment in the atmospheric column.

Consistent with the ETRN and DTRN profiles the upward cloud mass flux shows two peaks in Fig. 8b. One is around 950 hPa and the other around 250 hPa. The decrease of upward mass flux above 950 and below 350 hPa suggests an accumulation of cloud mass in that portion of the troposphere. A fraction of the mass sinks

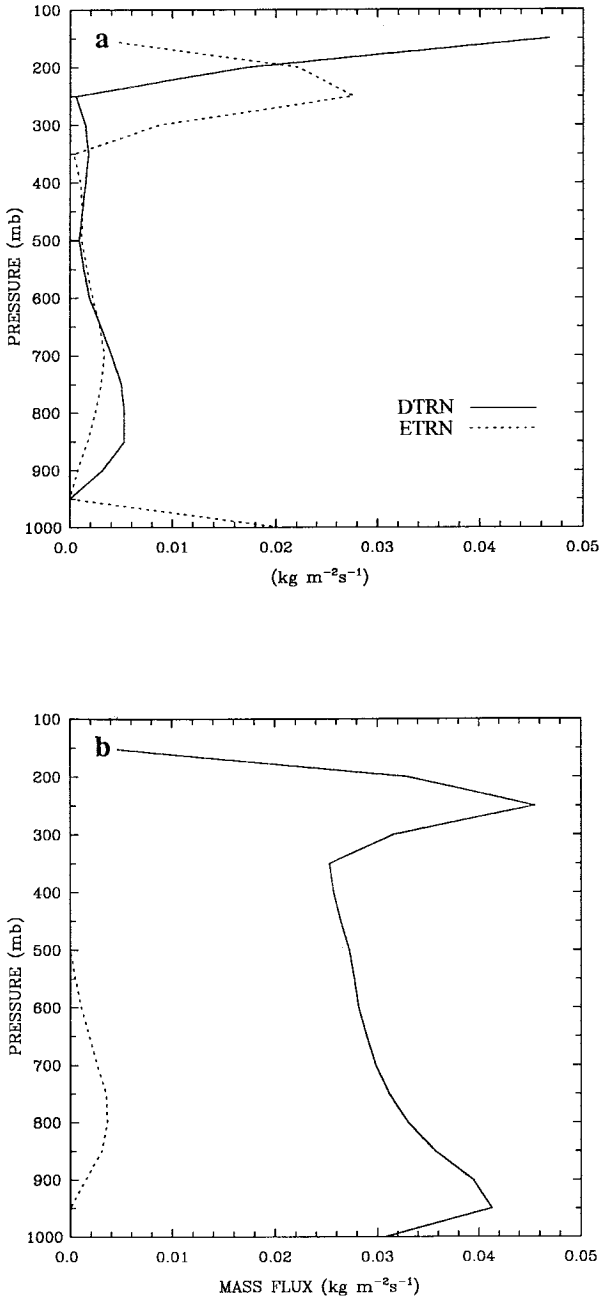


FIG. 8. (a) The averaged ETRN and DTRN rates of convection in the 1D model, and (b) upward (solid) and downward (dashed) convective mass fluxes (see text for definition of the terms).

as indicated by the downward mass flux. The increase of upward mass flux above 350 hPa corresponds to the increase of the ETRN rate in the saturated layer. The downward mass flux is smaller than the upward cloud mass flux, suggesting that more mixtures rise in finding their levels of neutral buoyancy. This seems natural when cloud dynamics are absent in a thermal model (Cotton and Anthes 1989).

### *b. Sensitivity analysis*

In this subsection, we present the results of the sensitivity of the parameterization to its three parameters, that is, precipitation efficiency ($\epsilon$), the probability for rain to fall outside of clouds and reevaporate ($\sigma$), and the vertical length scale of the mass shedding for thermals ($\lambda$). In the following discussions, we refer to the results presented in section 4a as the control results and present the sensitivity results to the three parameters in turn.

The dashed curve in Fig. 7 shows the relative humidity profile at equilibrium from an experiment in which we allowed 50% of the water condensate in a rising thermal to fall as precipitation. Compared to the control case, which used $\epsilon = 90\%$ (the solid curve in the figure), the major difference is a low relative humidity in the middle troposphere. When precipitation efficiency is smaller, a rising thermal has to hold more water condensate. Our analysis showed that there were fewer mixtures staying at the middle troposphere and more sinking to lower layers in this experiment than in the control run. This is partially due to the presence of water condensate in some of the mixtures and the negative effect of the condensate on the mixture's buoyancy. The dryness in the middle troposphere is a direct consequence of a reduced number of mixtures that would, otherwise, have stayed there and contributed to moistening those layers. Instead, the downward moving mixtures contributed to moistening the lower layers.

The other effect of a decrease of precipitation efficiency is the reduction of moistening lower layers by reevaporation of rain. The relative humidity profile in this experiment does not show this drying effect, however. This is because the drying effect is compensated to a large extent by increased moistening due to an increased number of sinking mixtures.

Model integrations with $\epsilon$ between 50% and 90% showed reasonable relative humidity profiles with a dry middle troposphere between the two curves in Fig. 7. Because of the balance between drying and moistening in the lower layers, there is no significant change of relative humidity in those layers.

Figure 9 shows the comparison of the relative humidity from two experiments that have different $\sigma$ values. The solid curve in Fig. 9 is for $\sigma = 0.30$, that is, 30% of the falling rain was available for reevaporation and the dashed curve is for $\sigma = 0.05$. The other model parameters used the same values as in the control case. From comparison of the two results we see that allowing a large fraction of rain to reevaporate results in higher relative humidity in most of the troposphere. The solid curve also has a minimum relative humidity around 400 hPa, which is higher than that of the dashed curve. This difference resulted because the moister environment in the middle atmosphere in this large reevaporation case favors more mixtures to rise to high layers from middle troposphere, resulting in elevating the height of the ma-

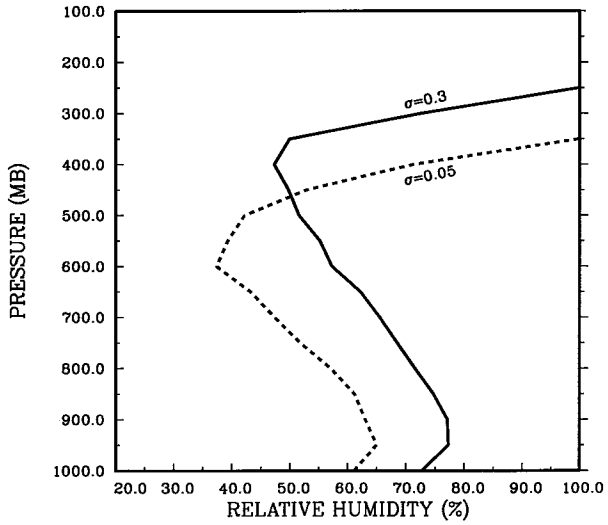


FIG. 9. Relative humidity profiles at equilibrium state from sensitivity experiments. The solid curve is for $\sigma = 0.30$ and the dashed curve for $\sigma = 0.05$.

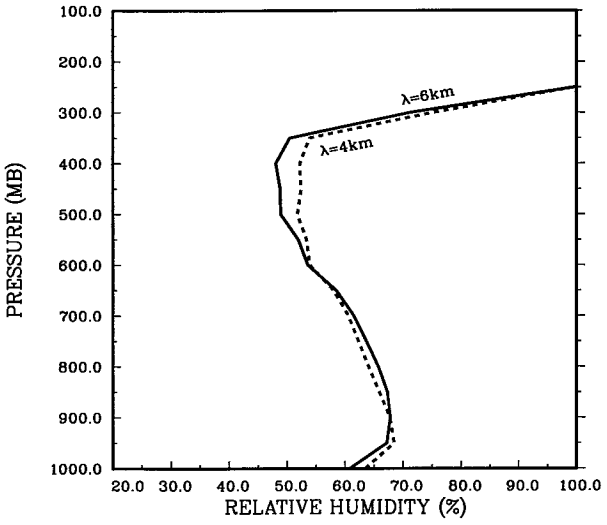


FIG. 10. Relative humidity profiles at equilibrium state from sensitivity experiments. The solid curve is for $\lambda = 6000$ m and the dashed curve for $\lambda = 4000$ m.

jor subsidence. The dashed curve in Fig. 9 shows that when a lesser amount of rain is allowed to reevaporate the middle and lower layers of the troposphere become dryer. Because $\sigma$ also represents the tilt of a convective cloud, the difference of the two curves in Fig. 9 suggests that a slantwise convection is more efficient to moistening the troposphere.

In Fig. 10 we present the equilibrium relative humidity profiles from two experiments that used different $\lambda$ values. The solid curve is for $\lambda = 6000$ m and the dashed one is for $\lambda = 4000$ m. Compared to the control result, both of these profiles show dryer layers in the lower troposphere and moister layers above 600 hPa. When $\lambda$ is larger, more mass of a thermal will be shed in middle and high layers of the troposphere [see (4)]. As a result, the middle and upper layers will be moister, and lower layers will be drier in a large $\lambda$ case than in a small $\lambda$ case. Some of these features are easily recognizable from comparisons of the results in Fig. 10 and the control result in Fig. 7. We found in analysis that there was more thermal mass shed in the layers between 600 and 350 hPa in the case of $\lambda = 4000$ m than in the case of $\lambda = 6000$ m. The latter has more mass shed in the layers above 300 hPa. Because of the model's rigid-lid upper boundary and the saturation above 300 hPa, the difference between the two cases is not shown above that pressure level and only the difference below the level is illustrated in Fig. 10.

In summary, these results from the 1D model show that the cumulus parameterization is in a reasonable range of sensitivity to its parameters.

## 5. Concluding remarks

We have presented a cumulus parameterization that applies a cloud model of intermittently rising thermals. In the cloud model, entrainment of environmental air and mixing of the entrained air with the air of a rising thermal occur at a thin layer near the top of the thermal. The mixing results in production of mixtures. These mixtures detach themselves from the rising thermal so that a further erosion to the buoyancy of the thermal by mixing is prevented, and the thermal is able to reach its level of neutral buoyancy as predicted by an adiabatic rising process (Warner 1970). In the parameterization, this process is equivalently considered as a rising thermal shedding portions of its mass to the layers that it passes by and the shed thermal mass mixing with environmental air to form mixtures. A convection episode consists of a sequence of thermal events occurring in an intermittent fashion. These thermal events consume the CAPE in the atmosphere. We assumed that the CAPE consumption by convection is in a quasi-balance with the CAPE production by grid-scale processes.

The differences between the current scheme and that of Raymond and Blyth (1986) and of Emanuel (1991) include the allowance of a varying number of saturated mixtures to result from the mixing process. This assumption affects the distribution of upward and downward cloud mass fluxes. Another feature of this scheme is the direct application of CAPE amount in determining the necessity of thermal development. We apply in the scheme an exponential profile for rising thermals to shed their mass in order to resemble the nearly exponential entrainment and mixing profile based on field experiments (Yanai et al. 1973; Blyth et al. 1987).

Except for the penetrative downdraft of sinking cloud mixtures whose level of neutral buoyancy is some distance below the levels where they form or in the boundary layer, no other types of penetrative downdrafts are included in this scheme. The downdraft of sinking mixtures can induce mass exchange between the bound-

ary layer and the layers above it. This mass exchange is an important process of convection in removing CAPE by replacing high moist static energy air in the boundary layer by low moist static energy air in the middle troposphere (Fritsch et al. 1976). An example demonstrating the effect of this process was presented in Hu and Randall (1995). The subsidence in the environment forced by convection also contributes in this CAPE-removal process. It can suppress the boundary layer depth and eliminate convective development (Suarez et al. 1983). Whereas these two processes are of fundamental importance in convective mass overturning and reducing boundary layer entropy, the penetrative downdraft driven by evaporative cooling and mechanical drag force associated with intense rainfall, and the one originating from interactions of convection and mesoscale circulation, play a prominent role in reducing boundary layer entropy (Fritsch et al. 1976; Frank and Molinari 1993; Raymond 1995), especially in mature stages of convection. Excluding these downdrafts is the major weakness of this scheme. We have shown some consequences from this weakness, for example, the differences in the boundary layer drying in the parameterized and diagnosed GATE results presented in section 3.

The sources of these downdrafts are different; the downdraft associated with rainfall originates within the convection, whereas the one driven by interactions of convection and mesoscale circulation enters convection from outside. Although observations showed that the center of intense rainfall in convective storms frequently coincides with the area of maximum downdrafts, analyses have revealed that such downdrafts are dynamically driven and very often originating from a rear-inflow entering convection from the middle troposphere [for a summary of these observations and analyses see Cotton and Anthes (1989)]. These channeled downward flows of air outside convection from middle troposphere provide a ''chamber'' *within* convection where evaporation of rain falling from mid- and upper troposphere is enhanced and so is the rainfall effect on surface outflows. These downdrafts bring massive low entropy air from the middle troposphere into the boundary layer in a short period of time. The CAPE is removed very efficiently through this channeled vertical redistribution of air masses of different entropy. Because of their intimate relationship, these two types of downdrafts, that is, the one associated with rainfall and the one from interaction of convection and mesoscale circulation, should both be included in a parameterization to describe the role of either of them in the development of convection.

A fundamental problem in doing so is how to determine their mass fluxes, particularly of the one originating from dynamic interactions. In different attempts (e.g., Johnson 1976; Cheng 1989; Raymond 1995), it has been assumed that the total downdraft mass flux of these processes was proportional to the updraft mass flux at the cloud base. However, many uncertainties exist in this simplified relationship (Raymond 1995). Until we understand the dynamic interactions of convection and its mesoscale environment, it would be difficult to present, in a physically consistent way, these penetrative downdrafts in a cumulus parameterization.

The results from our evaluations of the parameterization showed that the composites of parameterized convective heating and drying rates in the GATE period using this scheme are consistent with the composite rates diagnosed from the observations. The calculated convective precipitation rate compares reasonably well to the observed total precipitation rate at different regions of the easterly waves.

Evaluation of the scheme in a fully prognostic 1D model shows that this parameterization describes reasonably well the convective effects on temperature and moisture in the presence of grid-scale forcing processes. At the equilibrium state, the temperature and relative humidity profiles are comparable to the average profiles in the tropical atmosphere, except for an anvil layer above 300 hPa. The sensitivity analyses based on this 1D model further demonstrate the physical consistency of the scheme in parameterizing cumulus convection.

Although the evaluations of this parameterization using the GATE data and the 1D model showed consistent results and demonstrated the ability of this scheme to describe cumulus convection processes in the troposphere, the validity of these results is limited to the one-dimensional framework. In particular, the constant presence of a saturated anvil layer in the result suggests that these test results have been influenced to some degree by the dimension limitation of the 1D model. A multidimensional model with the presence of atmospheric dynamics, comprehensive radiation, and surface flux parameterizations is needed to fully evaluate this scheme.

The scheme's unique feature of allowing convective updrafts from multiple model layers in the troposphere and tracing their thermodynamic properties could be very useful for describing the role of cumulus convection in the distribution of atmospheric chemicals. The major concern in atmospheric chemistry models is the spatial and temporal distributions of the concentrations of various chemical species. In the vertical direction, the concentration profile of a chemical is primarily determined by convection. To accurately calculate the evolution of the vertical profile of a given chemical species with known sources and sinks, the convection scheme must provide the information of where and at what concentration a chemical species enters the convection and where and what amount of the chemical is discharged from the cumulus cloud. In addition, chemical reactions are important in production and destruction of some chemical compounds in the atmosphere. Many reactions occur or are catalyzed in the presence of liquid water, such as aqueous-phase chemical reactions. In calculating transport and concentration of chemical compounds that also simultaneously experience aqueous-phase reactions in convective clouds, a convection scheme must

describe the amount of liquid water as well as the concentration of the reactive chemicals in the cloud water. Knowing cloud water amount and the concentration of reactive chemical species in it, we can monitor the aqueous-phase chemistry in clouds and calculate to an improved accuracy the cloud's role in the production or destruction and the redistribution of chemical species in the atmosphere.

*Acknowledgments.* A major part of this work was developed at the State University of New York at Albany (SUNYA). I thank Dr. C. J. Walcek of SUNYA for support and for stimulating discussions. Thanks also go to Dr. K. M. Xu for his careful review and comments on an early draft of this manuscript, and to Drs. D. A. Randall and J. Y. Wang for making available to me the GATE observations and their GATE-derived larger-scale forcing quantities that have been used in the evaluations of the parameterization. I am grateful to Drs. J. Molinari, D. L. Zhang, S. Ghan, and S. E. Mudrick for helpful discussions. I thank the three anonymous reviewers whose critiques have stimulated deep thinking on many issues in convection and parameterization and led to improvements of this manuscript.

This work was supported by the Air Force Office of Scientific Research under Grant F49620-92-J-0018 and by the U.S. Department of Energy (DOE) ARM Program under Grant DE-FG02-92ER61364, both to SUNYA, and by the DOE ARM Program under Contract DE-AC06-76RLO 1830 to the Pacific Northwest National Laboratories.

## REFERENCES

Arakawa, A., and W. H. Schubert, 1974: Interaction of a cumulus cloud ensemble with the large-scale environment. Part I. *J. Atmos. Sci.,* **31,** 674–701.

Betts, A. K., 1973: Non-precipitating cumulus convection and its parameterization. *Quart. J. Roy. Meteor. Soc.,* **99,** 178–196.

——, 1982: Saturation point analysis of moist convective overturning. *J. Atmos. Sci.,* **39,** 1484–1505.

——, and M. J. Miller, 1986: A new convective adjustment scheme. Part II: Single column tests using GATE wave, BOMEX, ATEX and arctic air-mass data sets. *Quart. J. Roy. Meteor. Soc.,* **112,** 693–709.

Blyth, A. M., W. A. Cooper, and J. B. Jensen, 1988: A study of the source of entrained air in Montana cumuli. *J. Atmos. Sci.,* **45,** 3944–3964.

Bretherton, C. S., and P. K. Smolarkiewicz, 1989: Gravity waves, compensating subsidence, and detrainment around cumulus clouds. *J. Atmos. Sci.,* **46,** 740–759.

Chen, C., and H. D. Orville, 1980: Effects of mesoscale convergence on cloud convection. *J. Appl. Meteor.,* **19,** 256–274.

Cheng, M.-D., 1989: Effects of downdrafts and mesoscale convective organization on the heat and moisture budgets of tropical cloud clusters. Part I: A diagnostic cumulus ensemble model. *J. Atmos. Sci.,* **46,** 1517–1538.

Cotton, W. R., and R. A. Anthes, 1989: *Storm and Cloud Dynamics.* Academic Press, 883 pp.

Davies-Jones, R. P., 1974: Discussion of measurements inside high speed thunderstorm updrafts. *J. Appl. Meteor.,* **13,** 710–717.

Emanuel, K. A., 1983: The Lagrangian parcel dynamics of moist symmetric instability. *J. Atmos. Sci.,* **40,** 2368–2376.

——, 1991: A scheme for representing cumulus convection in large-scale models. *J. Atmos. Sci.,* **48,** 2313–2335.

——, J. D. Neelin, and C. S. Bretherton, 1994: On large-scale circulations in convecting atmospheres. *Quart. J. Roy. Meteor. Soc.,* **120,** 1111–1143.

Frank, W. M., and J. Molinari, 1993: Convective adjustment. *The Representation of Cumulus Convection in Numerical Models, Meteor. Monogr.,* No. 46, Amer. Meteor. Soc., 101–105.

Fritsch, J. M., and C. F. Chappell, 1980: Numerical prediction of convectively driven mesoscale pressure systems. Part I: Convective parameterization. *J. Atmos. Sci.,* **37,** 1722–1733.

——, ——, and L. R. Hoxit, 1976: The use of large-scale budgets for convective parameterization. *Mon. Wea. Rev.,* **104,** 1408–1418.

Heymsfield, A. J., P. N. Johnson, and J. E. Dye, 1978: Observations of moist adiabatic ascent in northeast Colorado cumulus congestus clouds. *J. Atmos. Sci.,* **35,** 1689–1703.

Hu, Q., and D. A. Randall, 1995: Low-frequency oscillations in radiative–convective systems. Part II: An idealized model. *J. Atmos. Sci.,* **52,** 478–490.

Jensen, J. B., P. H. Austin, M. B. Baker, and A. M. Blyth, 1985: Turbulent mixing, spectral evolution and dynamics in a warm cumulus cloud. *J. Atmos. Sci.,* **42,** 173–192.

Johnson, R. H., 1976: The role of convective-scale precipitation downdrafts in cumulus and synoptic-scale interaction. *J. Atmos. Sci.,* **33,** 1890–1910.

Kain, J. S., and J. M. Fritsch, 1990: A one-dimensional entraining/detraining plume model and its application in convective parameterization. *J. Atmos. Sci.,* **47,** 2784–2802.

Lord, S. J., 1982: Interaction of a cumulus cloud ensemble with the large-scale environment. Part III: Semi-prognostic test of the Arakawa–Schubert cumulus parameterization. *J. Atmos. Sci.,* **39,** 88–103.

——, and A. Arakawa, 1980: Interaction of a cumulus cloud ensemble with the large-scale environment. Part II. *J. Atmos. Sci.,* **37,** 2677–2692.

Ooyama, K., 1971: Convection and convective adjustment. V. A theory on parameterization of cumulus convection. *J. Meteor. Soc. Japan,* **49,** 744–756.

Randall, D. A., and J. Wang, 1992: The moist available energy of a conditionally unstable atmosphere. *J. Atmos. Sci.,* **49,** 241–255.

——, Harshvardhan, D. A. Dazlich, and T. G. Corsetti, 1989: Interaction among radiation, convection, and large scale dynamics in a general circulation model. *J. Atmos. Sci.,* **46,** 1943–1970.

Raymond, D. J., 1995: Regulation of moist convection over the West Pacific warm pool. *J. Atmos. Sci.,* **52,** 3945–3959.

——, and A. M. Blyth, 1986: A stochastic mixing model for nonprecipitating cumulus clouds. *J. Atmos. Sci.,* **43,** 2708–2718.

Reed, R. J., and E. E. Recker, 1971: Structure and properties of synoptic-scale wave disturbances in the equatorial western Pacific. *J. Atmos. Sci.,* **28,** 1117–1133.

Sarachik, E. S., 1978: Tropical sea surface temperature: An interactive one-dimensional atmosphere–ocean model. *Dyn. Atmos. Ocean,* **2,** 455–469.

Scorer, R. S., 1957: Experiments on convection of isolated masses of buoyant fluid. *J. Fluid Mech.,* **2,** 583–594.

Simpson, J., 1983: Cumulus clouds: Interactions between laboratory experiments and observations as foundations for models. *Mesoscale Meteorology—Theories, Observations and Models,* D. K. Lilly and T. Gal-Chen, Eds., Reidel, 399–412.

Stith, J. L., 1992: Observation of cloud-top entrainment in cumuli. *J. Atmos. Sci.,* **49,** 1334–1347.

Stull, R. B., 1984: Transilient turbulence theory. Part I: The concept of eddy-mixing across finite distance. *J. Atmos. Sci.,* **41,** 3351–3367.

Suarez, M. J., A. Arakawa, and D. A. Randall, 1983: The parameterization of the planetary boundary layer in the UCLA general circulation model: Formulation and results. *Mon. Wea. Rev.,* **111,** 2224–2243.

Taylor, G. R., and M. B. Baker, 1991: Entrainment and detrainment in cumulus clouds. *J. Atmos. Sci.,* **48,** 112–121.

Telford, J. W., 1975: Turbulence, entrainment and mixing in cloud dynamics. *Pure. Appl. Geophys.,* **113,** 1607–1684.

Thompson, R. M., S. W. Payne, E. E. Recker, and R. J. Reed, 1979: Structure and properties of synoptic-scale wave disturbances in the intertropical convergence zone of the eastern Atlantic. *J. Atmos. Sci.,* **36,** 53–72.

Tiedtke, M., 1989: A comprehensive mass flux scheme for cumulus convection in large-scale models. *Mon. Wea. Rev.,* **117,** 1779–1800.

Walcek, C. J., 1994: Cloud cover and its relationship to relative humidity during springtime midlatitude cyclone. *Mon. Wea. Rev.,* **122,** 1021–1035.

——, and G. R. Taylor, 1986: A theoretical method for computing vertical distributions of acidity and sulfate production within cumulus clouds. *J. Atmos. Sci.,* **43,** 339–355.

Warner, J., 1970: On steady state one-dimensional models of cumulus convection. *J. Atmos. Sci.,* **27,** 1025–1040.

Williams, E., and N. Renno, 1993: An analysis of the conditional instability of the tropical atmosphere. *Mon. Wea. Rev.,* **121,** 21–36.

Xu, K., and K. A. Emanuel, 1989: Is the tropical atmosphere conditionally unstable? *Mon. Wea. Rev.,* **117,** 1471–1479.

Yamasaki, M., 1975: A numerical experiment of the interaction between cumulus convection and large-scale motion. *Pap. Meteor. Geophys.,* **26,** 63–91.

Yanai, M., S. K. Esbensen, and J. Chu, 1973: Determination of bulk properties of tropical cloud dusters from large-scale heat and moisture budgets. *J. Atmos. Sci.,* **30,** 611–627.